The structural characterisation of HWCVD-deposited nanocrystalline silicon films

Bibhu P. Swain[a,b]

Nanocrystalline silicon (nc-Si) films were deposited by hot-wire chemical vapour deposition (HWCVD) in the presence of varying H_2 concentrations and their structural and interfacial character investigated by X-ray diffraction, small-angle X-ray scattering (SAXS) and Raman spectroscopy. The crystalline fraction was around 30–50% and the nc-Si crystallite size was in the range 20–35 nm. The SAXS results were analysed by Guinier plot, scaling factor, and correlation distance. The nc-Si grains displayed a mass fractal appearance, and the interfacial inhomogeneity distance was ~2 nm.

Key words: HWCVD, SAXS, Raman, XRD

Introduction

Nanocrystalline silicon (nc-Si:H) prepared as thin films by hot-wire chemical vapour deposition (HWCVD) at low substrate temperature has attracted much attention because of its potential application in low-cost, large-area electronic devices, such as flat panel displays and solar cells.[1] Hydrogen dilution of silane strongly affects the microstructure of silicon films so deposited.[2,3] Hydrogen-diluted nc-Si reportedly exhibits high stability against light soaking,[4,5] increases crystallite size and enhances mobility compared with amorphous silicon. Silane dilution can lead to a phase transition of silicon from an amorphous to a nanocrystalline and polycrystalline state.[4,5] However, macroscopic inhomogeneity in the growth direction, as well as in the growth plane of nc-Si, has been observed in HWCVD films.[6,7] Another aspect of nc-Si or poly-Si growth on glass and a-Si:H on graphite substrates in HWCVD processes is that nucleation of nanocrystalline material does not occur before the film thickness reaches 5 nm.[8] This means that the initial growth of the films, during the deposition of the first few nanometres, is structurally amorphous. Methods based on scattering phenomena are useful for studying material which is heterogeneous at a nanoscale,[9,10] especially those exhibiting nanocrystalline features. To calculate grain size and other characteristics of the crystallite interface, the following assumptions were made: (a) the scattering particles and their surrounding medium have uniform but different electron densities, (b) the volume fraction of the particles is low, and (c) the scattering particles are of an approximately known shape. Bingqing *et al.* analysed the influence of structural diversity and the size of spherical particles on the calculated size of distributions.[11]

The interpretation of the scattering effect from complex, disordered materials is notably simplified when fractal geometry is invoked to describe their structure. Much attention has been paid to the structural properties of nc-Si of HWCVD-deposited films derived from small-angle X-ray (SAXS) measurements,[8,12] but few papers describe the structural and interfacial nature of nanocrystalline silicon. This article reports on structural and interfacial studies of nanocrystalline silicon using both SAXS as well as X-ray diffraction (XRD) and Raman spectroscopy.

[a]Department of Physics, University of Cape Town, Private Bag, Rondebosch 7701, South Africa.
[b]Department of Metallurgical Engineering and Materials Science, Indian Institute of Technology, Mumbai, India.
E-mail: bibhuprasad.swain@gmail.com

Experimental details

Nc-Si:H films were formed on glass and crystalline Si substrates by hot-wire chemical vapour deposition under various H_2 dilution conditions in silane. Deposition parameters are shown in Table 1. XRD samples were studied with a vertical Philips X-pert (PANalytical) Model 3040/60 X-ray diffractometer. Raman spectra were recorded using a Labram-1 (Dilor-Jobin Yvon-Spex) spectrometer in backscattering mode with a spectral resolution of 2 cm^{-1}. The 488.0 nm (approximately 2.54 eV) line of an argon laser was used for excitation and the Raman scattered light was analysed using a charge-coupled device (CCD) camera for multi-channel detection. SAXS data were collected from a SAXSess Anton Parr, Model 3040/60 X-ray generator: PW 3830 PANalytical in-line collimating geometry using the transmission method at a wavelength of 0.154 nm. The experimental samples were deposited on Si(100) wafers, which were folded into two layers for signal enhancement. The X-ray intensity scattered at an angle of 2θ relative to the incident beam passing through the sample was obtained with a highly collimated beam. (The angle 2θ is usually converted into a scattering vector in terms of $h = 4\pi(\sin\theta)/\lambda$.) The X-ray intensity measured as a function of the scattering angle 2θ was corrected for absorption and scattering from the substrate. It was normalised by incident beam intensity I_o and film thickness to yield the normalised SAXS intensity, $I(h)$. After correction for background, data were analysed by Guinier plot, Porod plot, scaling behaviour and correlation distance.

Table 1. Deposition parameters of nanocrystalline silicon (nc-Si).

SiH_4 flow rate	1 sccm
H_2	15–35 sccm
Filament temperature	1800°C
Process pressure	100 mtorr
Substrate temperature	250°C
Substrate to filament distance	5 cm

Interpretation of SAXS results

Figure 1 shows SAXS intensities $I(q)$ obtained from nc-Si nanocrystals as a function of wavenumber ($q = (4\pi/\lambda)\sin\theta$). The scattering profiles have quantitatively similar features and can be divided into three regions on the q-axis by shape profile. The low q region (Region I; $q > 0.001$) gives an idea of grain size and shape of the nanocrystalline material. The sufficient condition for measuring radius of gyration is $q_{max}R_g < 1$. The Guinier approximation to determine radius of gyration is $I(q) = I_o \exp(q^2R_g^2/3)$. In the interface, the electron inhomogeneities are

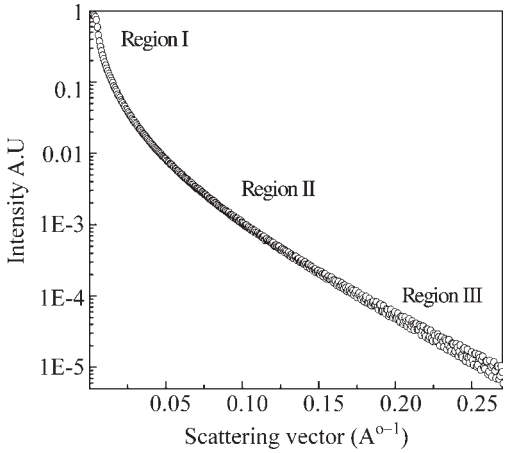

Fig. 1. SAXS plot of various nanocrystalline materials and structural information in relation to regions I–III.

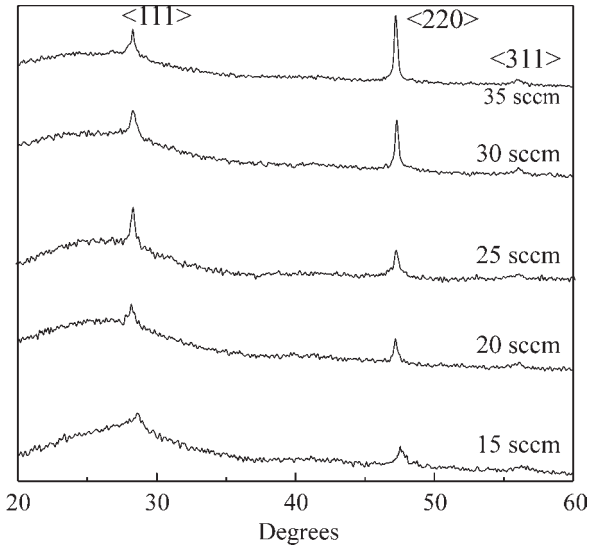

Fig. 2. XRD scans of different nc-Si films as a function of H_2 dilution.

different from those in a crystalline or purely amorphous network. The scattering vector corresponding to Region II ($0.05 < q < 0.15$) provides information about the interface and interfacial inhomogeneities of crystalline materials. Scaling behaviour and the Debye law are applicable to this region, where scattering exhibits self-similarity, based on fractals. Scaling law, the Power law or the presence of fractals gives a further idea of the distribution of nanocrystalline materials in a deposit, depending largely on cluster mobility. A Power plot is defined by the equation $I(q) = Aq^{-\alpha}$, where A is a constant related to the structural configuration of the nc-Si. α represents the fractal dimension and is equal to three for perfectly ordered materials. The material is considered to be mass fractal if $3 < \alpha < 0$ and surface fractal if $4 > \alpha > 3$. Debye theory provides a general description of an inhomogeneous system, from which scattering measurements can be used to indicate average electron density and the degree of correlation between two fluctuations as a function of their distance of separation. In Region III, correlation length is evaluated using the equation $I(q)^{-2/3} = Bq^2 + C$, such that the electron inhomogeneity distance is $\lambda = (B/C)^{1/2}$.[refs 13,14].

Results and discussion

The XRD spectra of silicon films prepared under different H_2 dilution conditions are shown in Figure 2. With increasing H_2 dilution, the appearance of three prominent peaks at about 28.4°, 47.28° and 56.8° indicates progressive crystallisation in the <111>, <220> and <311> directions, respectively. Figure 2 also shows that the full width at half maximum (FWHM) height of the XRD peak pattern decreased as the hydrogen dilution ratio increased. This indicated that the intermediate range order improves with H_2 flow rate. The average grain size of the experimental films is therefore estimated by the Debye-Scherrer formula to be 20–35 nm. The intensities, the positions and the FWHM of different XRD peaks of the experimental films are listed in Table 2. For clarity, the intensities were normalised to the (220) peak intensity. In the XRD data, the peak intensities, $I(hkl)$, of nc-Si:H films listed in Table 2 show that the $I_{(111)}/I_{(220)}$ ratio was in the range 0.68–2.11, whereas the $I_{(111)}/I_{(311)}$ ratio was in the range 4–5.9.

Figure 3(a) shows a typical Raman spectrum from a nc-Si:H film, which can be identified as four regions corresponding to two kinds of phonon modes—a longitudinal optical (LO) branch with a peak at ~400 cm^{-1} and a transverse optical (TO) mode.

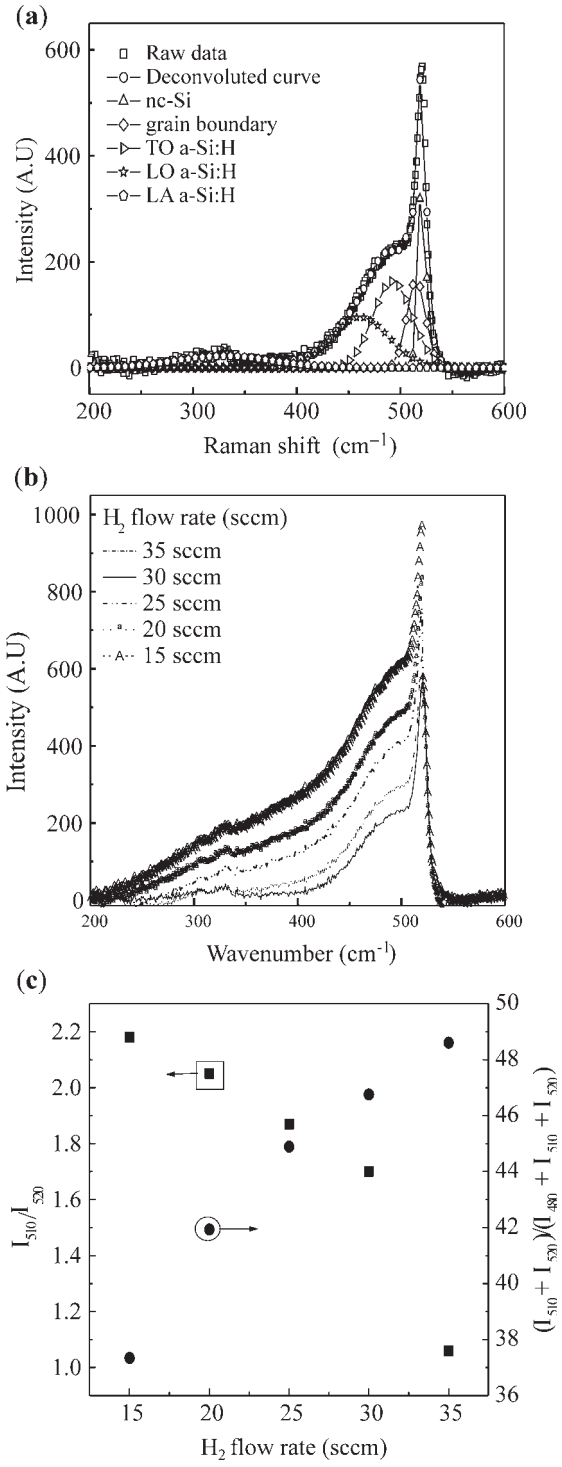

Fig. 3. (**a**) Deconvoluted Raman spectra; (**b**) Raman spectra of nc-Si; (**c**) I_{510}/I_{520} (■) and $(I_{480}+ I_{520})/(I_{480}+ I_{510} + I_{520})$ (●) ratio of experimental films deposited by HWCVD under different hydrogen dilution conditions. TO, transverse optical; LO, longitudinal optical; a-Si, amorphous silicon; nc-Si, nano-crystalline silicon.

Further, the TO band can be further divided into three parts: a transverse optical branch (TO_1) with a peak at 480 cm^{-1} from the amorphous Si contribution, a transverse optical mode (TO_1) at about 510 cm^{-1} from the contribution of Si interfacial nanocrystals, and another transverse optical mode (TO_2) at 520 cm^{-1} from the contribution of Si core nanocrystal. These modes are depicted in Figure 3(a), from which the LO and a-TO, TO_1 and TO_2 branches can be seen to fit well to a Gaussian distribution. This implies that every fitted line can be approximately repre-

Table 2. Details of XRD results.

H_2 dilution (sccm)	(111)			(220)			(311)		
	Position (°)	FWHM (°)	Intensity	Position (°)	FWHM (°)	Intensity	Position (°)	FWHM (°)	Intensity
15	28.59	1.26	100	47.55	0.512	99.3	57.91	0.83	25.56
20	28.31	0.51	100	47.19	0.29	88.6	56.1	0.48	18.9
25	28.29	0.44	100	47.25	0.37	68.45	56.1	0.93	11.71
30	28.27	0.41	51.5	47.29	0.29	100	56.04	0.56	12.85
35	28.27	0.25	39.13	47.2	0.29	100	55.9	0.77	6.8

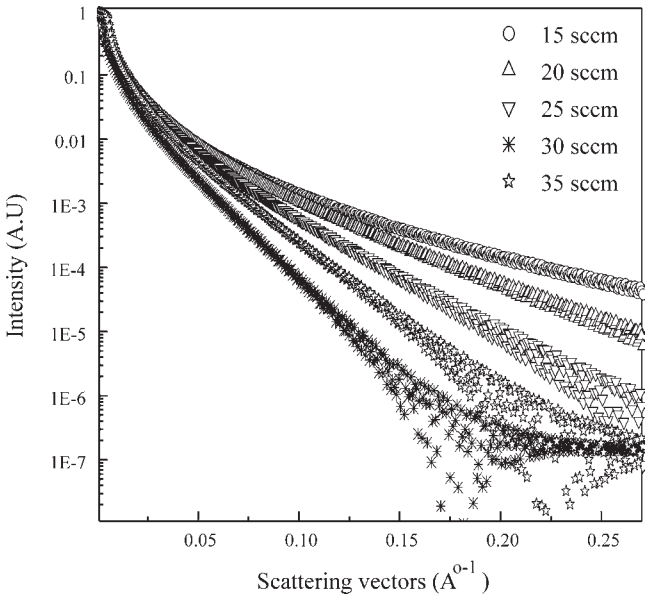

Fig. 4. SAXS plots of different nc-Si films as a function of H_2 flow rate.

sented by every mode deconvoluted from an experimental Raman spectrum.[15]

The crystalline fraction (X%) is estimated from the formula $\delta I_c/(I_a + I_c) = (I_{510} + I_{520})/(I_{475} + I_{510} + I_{520})$, where I_{480} is the amorphous silicon peak intensity and I_{520} is the Raman scattering for crystalline silicon. Figure 3(b) shows micro-Raman spectra of nc-Si:H as a function of H_2 flow rate. An obvious effect of increasing the H_2 concentration is the shift of the Si TO band towards higher frequency as depicted by the dashed line. The peak intensity observed at 517 cm^{-1} corresponded to a 15 sccm H_2 flow rate, whereas it shifted to 519 cm^{-1} for a flow rate of 35 sccm; the corresponding crystalline fractions were 37% and 49%. Also clearly indicated is that H_2 dilution suppresses the amorphous fraction in the nc-Si network and increases the crystalline fraction. It is the growth and the shift of the second TO band relative to the 475 cm^{-1} band that causes the peak of the overall TO band to shift to higher frequencies. This shift indicates increasingly ordered structure as found in H_2-diluted films[16] and is consistent with recent calculations which have depicted an increase of the TO peak frequency with a decrease of the mean bond-angle deviation.[20] Figure 3(c) shows the I_{510}/I_{520} and $(I_{510}+ I_{520})/(I_{480} + I_{510} + I_{520})$ ratios as a function of H_2 flow rate. It indicates that the grain boundary contribution was reduced with increase in H_2 dilution in the nc-Si network. This indicated that the thickness of the inhomogeneous layer was almost constant in the nc-Si:H films. The I_{510}/I_{520} ratio indicates surface scattering in relation to scattering by the crystalline core in the experimental films. This ratio decreased from 2.2 to 1.1, reflecting a reduction in interfacial inhomogeneity with hydrogen dilution.

Figure 4 illustrates ln(I) in relation to normalised SAXS intensity as a function of H_2 flow rate. The slope of the SAXS intensity

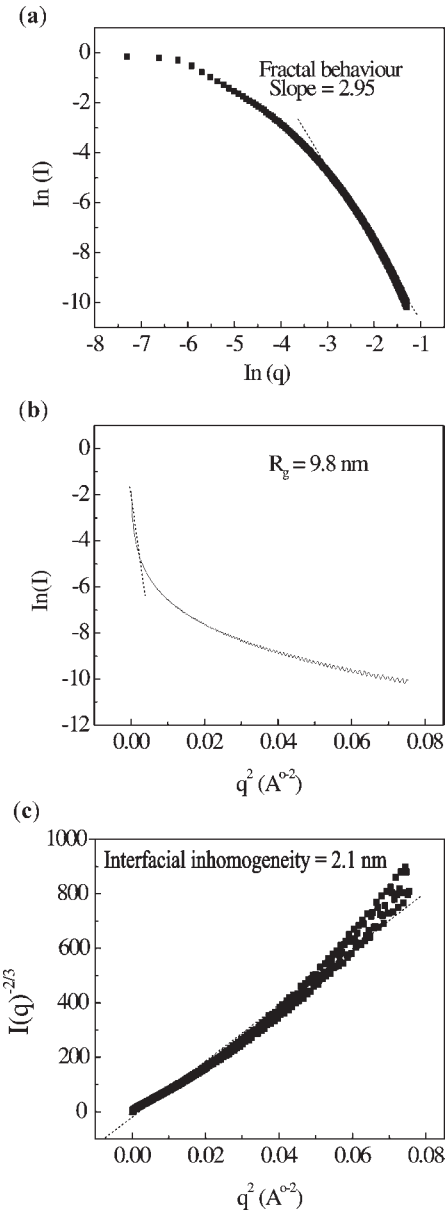

Fig. 5. (**a**) ln(I) versus ln(q) for scaling behaviour; (**b**) ln(I) versus q^2 as a Guinier plot; (**c**) $I^{-2/3}$ versus q^2 as a Debye plot. The sample of nanocrystalline silicon in each case was deposited at a H_2 flow rate of 15 sccm.

decreased progressively with increase in flow rate.

The splitting SAXS scattering at higher q values was more prominent and this was due to scattering from a nanocrystalline silicon surface. Figure 5(a) shows that ln(I) versus ln(q) exhibits power law behaviour for a hydrogen flow rate of 15 sccm, as in a two-phase system where nanocrystalline silicon is surrounded by an amorphous a-Si:H network. At $q > 0.03$ Å, the nanocrystalline silicon indicates enhanced order; a slope of more than three

Table 3. SAXS structural parameters of nc-Si:H films.

H_2 dilution (sccm)	Crystallite size (nm)	Crystalline fraction (%)	Radius of gyration (Å)	Scaling factor (mass fractal)	Correlation distance (Å)
15	20.9	37.3	9.8	2.95	2.1
20	26.0	41.9	10.2	2.85	2.1
25	28.1	44.9	11.2	2.79	1.9
30	32.2	46.8	12.4	2.75	2.0
35	33.8	48.6	12.9	2.77	1.9

indicates surface fractal characteristics. Table 3 shows the scaling factor for films deposited at different H_2 flow rates. This result suggests that this particular crystallite network consists of fractal clusters ($D_m = 2.95 \pm 0.02$) of particles with smooth surfaces. Figure 5(b) is a Guinier plot, in which the slope is taken over the range where $R_g q < 1$. R_g, the radius of gyration of the clusters, varies from 9.8 nm to 12.9 nm as H_2 dilution increases from 15 to 35 sccm. Assuming the presence of uniform spheres, the corresponding cluster diameter is equal to $2R_g(5/3)$.[0.5] Grain size increases from 25 to 33 nm and corresponds with crystallite size determined by XRD. Figure 5(c) shows a Debye plot as a measure of the mean inhomogeneity in the experimental materials. The inhomogeneity distance is approximately 2 nm for a H_2 flow rate in the range 15–35 sccm.

Conclusion

These various studies based on SAXS, XRD and Raman spectra of nc-Si:H films deposited by HWCVD techniques under varying hydrogen dilution conditions, indicate that crystallite size and crystalline fraction increased from 20 nm to 35 nm and from 40% to 49%, respectively. Crystallites of nanocrystalline silicon displayed a mass fractal nature and interfacial inhomogeneities were of the order of 2 nm in size. The relative effect of grain boundaries in relation to grain size declined in films deposited with reduced H_2 flow rate.

This paper has been presented at Nanoafrica 2006, University of Cape Town. The author gratefully acknowledges D.T. Britton and M. Harting, Department of Physics, University of Cape Town, for financial support and helpful discussions.

Received 30 January 2007. Accepted 2 March 2009.

1. Brühne K., Schubert M.B., Köhler C. and Werner J.H. (2001). Nanocrystalline silicon from hot-wire deposition—a photovoltaic material? *J. Non-Cryst. Solids* **395**, 163–168.
2. Pan B.C. and Biswas R. (2004). Simulation of hydrogen evolution from nano-crystalline silicon. *J. Non-Cryst. Solids* **333**, 44–47.
3. Tamir S. and Berger S. (2000). Electroluminescence and electrical properties of nano-crystalline silicon. *Mater. Sci. Engng. B.* **69–70**, 479–483.
4. Ziegler Y., Daudrix V., Droz C., Platz R., Wyrsch N. and Shah A. (2001). More stable low gap a-Si:H layers deposited by PE-CVD at moderately high temperature with hydrogen dilution. *Solar Ener. Mater. Solar Cell.* **66**, 413–419.
5. Bauer S., Schröder B. and Oechsner H. (1998). The effect of hydrogen dilution on the microstructure and stability of a-Si:H films prepared by different techniques. *J. Non-Cryst. Solids* **227–230**, 34–38.
6. Koh J., Fujiwara H., Collins R.W., Lee Y. and Wronski C.R. (1998). Microstructural evolution of a-Si:H prepared using hydrogen dilution of silane studied by real time spectroellipsometry. *J. Non-Cryst. Solids* **227–230,** 73–77.
7. Cabarrocas R.I, Layadi N., Drevillon B. and Solomon I. (1996). Microcrystalline silicon growth by the layer-by-layer technique: long term evolution and nucleation mechanisms. *J. Non-Cryst. Solids* **198–200**, 871–874.
8. Zhu M., Guo X., Chen G., Han H., He M. and Sun K. (2000). Microstructures of microcrystalline silicon thin films prepared by hot wire chemical vapor deposition. *Thin Solid Films* **360**, 205–212.
9. Gracin D., Juraic K., Dubcek P., Gajovic A. and Bernstorff S. (2006). The nano-structural properties of hydrogenated a-Si and Si–C thin films alloys by GISAXS and vibrational spectroscopy. *Appl. Surf. Sci.* **252**, 5598–5601.
10. Gracin D., Juraic K., Dubcek P., Gajovic A. and Bernstorff S. (2005) Analysis of the nano-structural properties of thin film silicon–carbon alloys. *Vacuum* **80**, 98–101.
11. Zhou B., Liu F., Gu J., Zhang Q., Zhou Y. and Zhu M. (2006). Nano-structure in micro-crystalline silicon thin films studied by small-angle X-ray scattering. *Thin Solid Films* **501**, 113–116.
12. Ray P.P., Gupta N.D., Chaudhuri P., Williamson D.L., Vignoli S. and Longeaud C. (2002). Properties of Si:H thin films deposited by rf-PECVD of silane–argon mixtures with variation of the plasma condition. *J. Non-Cryst. Solids* **299–302**, 123–127.
13. Martin J.E. and Hurd A.J. (1987). Scattering from fractals. *J. Appl. Cryst.* **20**, 61–78.
14. Teixeira J. (1988). Small-angle scattering by fractal systems. *J. Appl. Cryst.* **21**, 781–785.
15. Tsu D.V., Chao B.S., and Ovshinsky S.R., Guha S. and Yang J. (1997). Effect of hydrogen dilution on the structure of amorphous silicon alloys. *Appl. Phys. Lett.* **71**, 1317–1319.
16. Koh J., Ferlauto A.S., Rovira P.I., Wronski C.R. and Collins R.W. (1999). Evolutionary phase diagrams for plasma-enhanced chemical vapor deposition of silicon thin films from hydrogen-diluted silane. *Appl. Phys. Lett.* **75**, 2286–2288.